ASTRONOMY & ASTROPHYSICS
SUPPLEMENT SERIES

Astron. Astrophys. Suppl. Ser. **123,** 209-218 (1997)

A new radial velocity curve for the RS CVn star σ Gem*

Constraints on its physical parameters

R. Duemmler, I.V. Ilyin, and I. Tuominen

Department of Geosciences and Astronomy, University of Oulu, Linnanmaa, P.O. Box 333, FIN–90571 Oulu, Finland

Received July 25; accepted September 25, 1996

Abstract. 26 high quality radial velocity measurements of the RS CVn star σ Gem taken in 1993, 1994, and 1995[1] are used in combination with older measurements to fit a new radial velocity curve. Essentially, the orbital parameters given by Bopp & Dempsey (1989) are confirmed. However, the orbit turns out to be circular. σ Gem is known as a single–lined binary, and also in the new spectra no trace of the secondary is found. However, combining the orbital with rotational parameters, constraints on the fundamental parameters can be found: the inclination, the radius and the two masses. The inclination is high; the mass of the primary seems to be normal for a K1 giant, its radius, however, seems to be too small.

Key words: stars: spectroscopic — stars: fundamental parameters — binaries: stars individual: σ Gem

1. Introduction

σ Gem (75 Gem = HR 2973 = HD 62044; $V \approx 4\overset{\mathrm{m}}{.}2$) belongs to the class of RS CVn stars. These stars are close binaries with usually one evolved component (sub–giant or giant) with signatures of strong activity in one or both components. σ Gem is classified as K1 III and as a single–lined binary. These and a number of further parameters of the star are listed in Strassmeier et al. (1993, Star No. 73). For a RS CVn star, it has an untypically long period of 19.6 days, a fact that might lead to some other, untypical properties (Hatzes 1993).

The latest orbit calculations were done by Bopp & Dempsey (1989). They found a marginally eccentric orbit, but note that the orbit may be circular. They remark that there is no significant change of the orbit over the time span available to them (1902–1988).

Twenty–six new radial velocities (RVs) were obtained in 3 runs in 1993, 1994 and 1995. The SOFIN high resolution echelle spectrograph was used, yielding additional to the high resolution high S/N spectra (typically S/N > 200).

The new radial velocities offer some prospects: first, they extend the time base of RVs of σ Gem by another 7 years; thus, they allow for further improvement of the orbital period. They are far more accurate than any previously published radial velocities (see below). Thus, they are used to check the non-circularity of the orbit and to determine accurate values for all other orbital parameters. Furthermore, due to the high resolution and the high S/N ratio the spectra might allow for the detection of spectral lines belonging to the secondary. Additionally, some old RVs not used by Bopp & Dempsey are supplemented. Altogether, a new orbit determination is worthwhile, especially as a preparation of the spectra for surface (Doppler) imaging, where the shifts due to the orbital motion and the line profile distortions due to star spots need to be separated with high accuracy. Surface images from the SOFIN spectra will be discussed in a forthcoming paper.

2. Observations and reductions

For the purpose of surface imaging, very high–resolution (about 170 000 at 6173 Å), high S/N spectra (about 200 − 300) were obtained with the high–resolution echelle spectrograph SOFIN (Tuominen 1992) at the 2.56 m Nordic Optical Telescope (NOT) at Roque de los Muchachos Observatory, La Palma, Spain. The high resolution optical camera was used. The entrance slit width of 32 μm is adjusted to give a resolution element of about 2 pixels FWHM, corresponding to $0\overset{''}{.}23$ on the sky. The spectra were recorded with an Astromed–3200 CCD

Send offprint requests to: R. Duemmler;
e-mail: Rudolf.Duemmler@oulu.fi

* based on observations collected at the Nordic Optical Telescope (NOT), La Palma, Spain.

[1] Table 1 is also available in electronic form at the CDS via anonymous ftp to cdsarc.u-strasbg.fr (130.79.128.5) or via http://cdsweb.u-strasbg.fr/Abstract.html

camera (Mackay 1986) equipped with an EEV P88200 UV–coated 1152 × 770 CCD with a pixel size of 22.5 μm and operating at the optimal working temperature of 150 K. Three observing runs for σ Gem were conducted in late 1993, 1994 and 1995. Typical integration times were 30–40 minutes.

The reductions of the echelle spectra used the 3A–software package (Acquisition, Archiving and Analysis; Ilyin 1996).

The reductions involved the usual procedures of cosmic spike removal, bias subtraction, flatfielding, subtraction of scattered light, extraction of the curved echelle orders and wavelength calibration. The result is for each order the intensity normalized to the local continuum vs. heliocentric wavelength.

Two steps deserve a more detailed description. Flatfielding uses summed, merged flatfields, i.e. the slit height is so large that the orders of the flatfield spectra overlap; many of those images are summed in order to improve the S/N ratio in the flatfields. Fringing is usually of very low amplitude or absent. In some cases, however, an ordinary flatfield image is available, taken with the same parameters and immediately before or after the stellar exposure, which, after flatfielding and filtering to improve S/N and retain only the fringes, can be used to correct the corresponding stellar spectrum for fringing.

In order to obtain the highest possible accuracy in the wavelengths, a *two–dimensional* dispersion curve is determined from the Thorium–Argon comparison spectrum; this has the main advantage to use many comparison lines from many orders, as opposed to the sometimes very low number of comparison lines available in one individual echelle order. The determination proceeds as follows:

- Many orders from the comparison spectrum image are extracted in the same way as the orders from the stellar spectrum image and the backgrounds are subtracted.
- The positions of the comparison lines are determined by fitting of Gaussians.
- The wavelengths are identified semi–automatically using the Kitt–Peak Atlas for the Thorium–Argon–spectrum (Willmarth 1987).
- After determination of the two–dimensional positions $(x_i,\ y_i)$ for many $(100 - 200)$ comparison lines, all are transformed into one master order, using the $k\lambda$–law, i.e.

$$\lambda_0 = \lambda_i \frac{k}{k_0}, \tag{1}$$

  where k is the order number in which the line with wavelength λ_i has been measured and (k_0, λ_0) correspond to the master order.
- The merging of all lines in the master order is subsequently optimized according to the model:

$$\begin{aligned} p_i &= y_i \sin\alpha_i + x_i \cos\alpha_i \\ \alpha_i &= a + b\, x_i. \end{aligned} \tag{2}$$

  The first equation describes the rotation of the CCD rows with respect to the lines perpendicular to the dispersion direction. The rotation angle, and thus the curves $k\lambda$ = const., are modified due to the optical distortions as described by the second equation. It was found, that this simple model works very well for our spectrograph, where the incident and diffracted beams are in the same plane. a and b are optimized by minimizing the χ^2 of all merged comparison lines from a single polynomial describing the dispersion curve of the master order.
- The polynomial is then transported along the lines $k\lambda$ = const. into each of the orders of the original image, yielding a dispersion curve for each of them that is based on all the comparison lines distributed all over the original two–dimensional image.
- Finally, telluric lines are used to establish the accurate wavelength zero point, correcting for tiny geometrical shifts between the comparison and stellar images due to bending of the spectrograph.

The accuracy of the RVs is determined by the following factors:

- The *accuracy of the dispersion curve*: typically, about 150 comparison lines are taken into account. The dispersion curve within the master order is described by a polynomial of 2nd degree; the rms deviation of the lines from the final fit is generally about 2 mÅ at 6165 Å or 0.1 km s^{-1}. Since due to the large number of comparison lines used the error of the coefficients is much less than that, we conclude that the statistical error of the dispersion curve is negligible.
- The *stability of the RV across the chip*: any systematical error of the two–dimensional dispersion curve should show up as a systematical variation of the RV across the different orders. This was checked in the spectrum of the RV–standard β Oph: the RV is stable across the chip to within 0.03 km s^{-1}. Also for σ Gem with its much broader lines due to fast rotation the RV is stable to better than 0.1 km s^{-1}.
- The *accuracy of the wavelength zero point*: Each spectral image is shifted geometrically with respect to the image containing the comparison spectrum. Strong atmospheric O_2 and H_2O lines are used to establish the wavelength zero point. The standard wavelengths are taken from the solar catalogue by Pierce & Breckinridge (1973). In the present spectra, three different orders are available, each containing enough atmospheric lines to establish independently the wavelength zero point. They prove that there is no significant systematic variation of the shift across the image and allow an error estimate for the shift. Typically, the shift is determined with an accuracy of 0.1 to 0.2 CCD pixels. Since in echelle spectra in a good first approximation the dispersion is proportional to the wavelength this uncertainty transforms to a

systematic error of the RV from the whole image of about 0.1 to 0.2 km s^{-1}.

– The *accuracy of the template's RV*: The RV of σ Gem is measured by cross–correlating the wavelength region around 6175 Å with the same region of a spectrum of β Oph (K2 III), taken with the same equipment and reduced in the same way. The spectrum has been filtered to mimic the rotational broadening in the σ Gem spectra. β Oph is a radial velocity standard (see Astronomical Almanac 1995), a candidate for a list of primary standards; we can thus assume that both the constancy and the value of its RV are established to high accuracy. According to the Astronomical Almanac (1995) its RV = (-12.0 ± 0.1) km s^{-1}.
– The *accuracy of the cross–correlation*: At present, this cannot be determined independently. Therefore, we adopt an error of another 0.1 km s^{-1} from this procedure.

If we assume these error sources to be independent and add up the variances from the different contributions, the final RV–error is about 0.3 km s^{-1}. Note that although all the above error sources are also present in the template spectrum only the second to last source enters into the RV–error of σ Gem, since the literature value for the RV of β Oph is used to determine the RV from the cross–correlation.

The RVs measured from the SOFIN spectra are given in Table 1.

3. The radial velocity curve

3.1. The full data set

The radial velocities measured from the SOFIN spectra (Table 1) are supplemented by older measurements from the following sources (N is the number of RVs given):

Abt (1970), $N = 1$
Bopp & Dempsey (1989), $N = 110$
includes 19 values from Harper (1935)
Eker (1986), $N = 9$
Harper (1914), $N = 38$
Harper (1935), $N = 21$
includes 2 values from Harper (1914)
5 values from Moore (1928),
4 of which are revised from Reese (1903)
4 values from Jones (1928),
also listed by Lunt (1919).

An obvious misprint in one JD given by Harper (1935) has been corrected. Eker's RVs were not published before; he kindly made them available to us, and they are given in Table 2. The total number of RVs is thus 187 and the time interval covered by them ranges from 1902 to 1995.

The data are weighted, with the weight of an individual RV being the inverse of its variance. Since no individual errors for the older RVs are known, for each set of data a common mean standard deviation is adopted:

Table 1. The radial velocities (RVs) measured from the SOFIN spectra. The heliocentric Julian date is given for mid-exposure. A typical error of the individual RV is 0.3 km s^{-1}

date [dd.mm.yy]	HJD −2400000.0	RV [km s^{-1}]
26. 09. 93	49256.7404	39.5
27. 09. 93	49257.6758	28.7
28. 09. 93	49258.7281	19.6
29. 09. 93	49259.7266	13.6
30. 09. 93	49260.7196	10.0
02. 10. 93	49262.7492	12.3
03. 10. 93	49263.7351	20.5
04. 10. 93	49264.7213	27.5
05. 10. 93	49265.7339	40.9
06. 10. 93	49266.7125	51.8
03. 11. 93	49294.7532	52.1
13. 11. 94	49669.7733	24.9
14. 11. 94	49670.6763	17.8
15. 11. 94	49671.6859	12.1
16. 11. 94	49672.6892	10.0
18. 11. 94	49674.6961	15.9
18. 11. 94	49674.7486	16.3
19. 11. 94	49675.7660	24.1
21. 11. 94	49677.6992	44.4
22. 11. 94	49678.6537	54.5
15. 12. 94	49701.6142	78.9
15. 12. 94	49701.6714	79.1
18. 12. 94	49704.5654	70.3
20. 12. 94	49706.6310	50.2
01. 12. 95	50052.7725	69.8
02. 12. 95	50053.7750	75.9
03. 12. 95	50054.7828	77.5
04. 12. 95	50055.7708	76.8
05. 12. 95	50056.7620	73.5

Table 2. The previously unpublished RVs measured by Eker. The measurement procedure and the interpretation is given in Eker (1986). He estimates the RV error to be 0.5 km s^{-1}

date [dd.mm.yy]	HJD −2400000.0	RV [km s^{-1}]
23. 02. 84	45753.6713	11.6
29. 02. 84	45759.6119	71.5
03. 03. 84	45762.7217	78.2
07. 03. 84	45766.6354	48.8
09. 03. 84	45768.7292	23.8
23. 03. 84	45782.7120	75.7
26. 03. 84	45785.7147	50.8
01. 04. 84	45791.7071	11.3
06. 04. 84	45796.6927	50.2

Bopp & Dempsey (1989) estimate their RV–errors to be $0.9\,\mathrm{km\,s^{-1}}$, and they assign to the data given by Harper (1914, 1935) a weight of 0.5 with respect to their own measurements. This translates to a standard deviation of $1.3\,\mathrm{km\,s^{-1}}$, which is adopted here and also used for the RV given by Abt (1970). Eker (1986, see Table 2) gives an error of $0.5\,\mathrm{km\,s^{-1}}$. We estimate the error of the SOFIN RVs to be $0.3\,\mathrm{km\,s^{-1}}$(see above).

3.2. The fit and error determination

The data consisting of triples (t_i, RV_i, w_i) with the weights w_i are fitted (least–squares fit) by the function

$$\mathrm{RV}(t) = \gamma + K\,(\cos(v+\omega) + e\cos\omega), \tag{3}$$

(see e.g. Heintz 1978 for the derivation and the meaning of the symbols).

The parameters are determined with a non–linear least–squares fit using the simplex–algorithm (e.g. Caceci & Cacheris 1984; Press et al. 1994).

As an additional parameter derived from the fit–parameters, we compute the period in the rest frame of the system (corrected for the time dilation in the inertial frame moving with the velocity γ with respect to the sun, and to the increasing light travel–time between periastron passages due to γ). We use P_{rest} in the computation of $a\sin i$ and $f(m)$.

There are two ways to determine standard deviations for the fit–parameters.

1. The *formal error* of any fit–parameter p is given by
$$\sigma_{\mathrm{p}}^2 = 2\left(\frac{\partial^2\chi^2}{\partial p^2}\right)^{-1} \tag{4}$$
(Bevington 1969) with the derivatives taken at the minimum of χ^2. With the fit–parameters and their formal errors known, the errors of the derived parameters can be obtained by the usual error propagation.
2. The *bootstrap errors* (see e.g. Efron & Tibshirani 1993) are computed from the actual residuals of the measurements from the fit. B bootstrap samples are constructed by randomly selecting from the residuals of the N real measurements N residuals, with replacement, and adding them to the computed RVs using the best fit parameters. Since the residuals of measurements having low weight are on average larger than those of measurements having high weight, each residual picked is accompanied by its original weight. For each set of these new "measurements" a fit of the RV curve is performed, resulting in a new set of fit–parameters and derived parameters. For large B the parameter errors are given by the standard deviations of the bootstrap parameters (both fit–parameters and derived ones) from their values obtained from the set of real measurements.

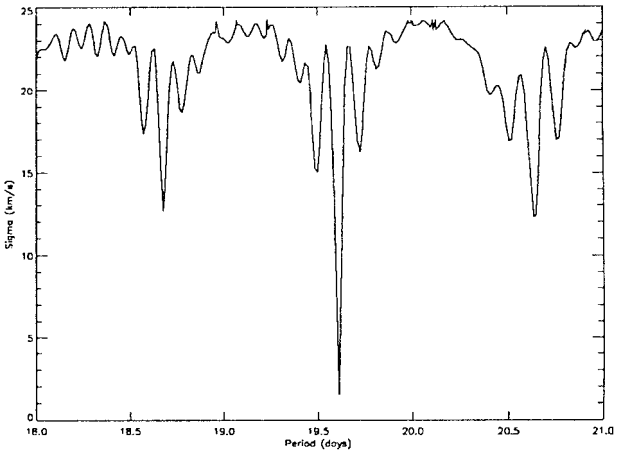

Fig. 1. Periodogram of the RV measurements of σ Gem. The only significant period is at 19.604471 days

3.3. The period search

Assuming the orbit to be circular, i.e. fixing $e = 0$ in the fits, and removing the last 3 measurements from Table 1 (see Sect. 3.4), the best orbital period was searched in the interval 18.0 to 21.0 days.

Figure 1 shows the periodogram obtained by varying the start value of the period in fits of RV curves to the data set. The plot gives the standard deviation σ_1 of an individual measurement of mean weight from the fit vs. the period. It is obvious that there is only one period close to the value given by Bopp & Dempsey (1989); all other minima have σ_1 exceeding $10\,\mathrm{km\,s^{-1}}$.

3.4. The radial velocity curve of σ Gem

The results of four different fits of radial–velocity curves are given in Table 3. Except for Solution 4, all allow for a non–zero eccentricity of the orbit. The formal parameter errors are only given for Solution 1: one can see that in most cases the formal and the bootstrap errors are very close to each other. The main exception is ω which has a very large bootstrap error. The bootstrap error is certainly more realistic due to the very small eccentricity. This relation between the formal and the bootstrap errors is the same for all fits; only the (more reliable) bootstrap errors are therefore given in the following.

A forced circular fit to all measurements excluding the last 3 SOFIN measurements (see below) yields a slightly different period than that given in Solution 1:

$$P = (19.604471 \pm 0.000022) \quad \text{days}, \tag{5}$$

which is adopted as the final period. This period is kept fixed in fits leading to Solutions 2–4, because the limited time–coverage of the data sets used for them does not allow a reliable determination of the period.

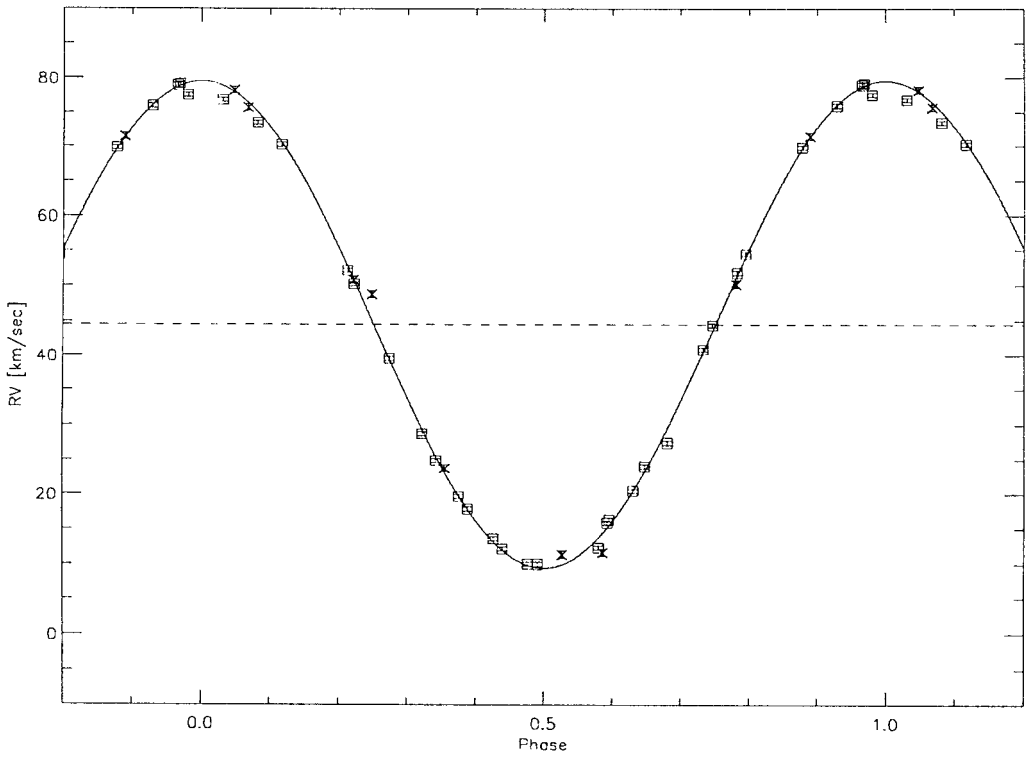

Fig. 2. The SOFIN measurements (squares) and Eker's measurements (crosses) with the radial velocity curve of Solution 4

The eccentricity of the orbital solution 1 is only half of what Bopp & Dempsey (1989) got. Solutions 2 and 3 are obtained with the aim to establish the significance (or otherwise) of this eccentricity. Only the data sets having the smallest velocity errors, i.e. the SOFIN and Eker's data sets (Table 1 and Table 2), are used. Solution 2 uses all of these data. The eccentricity has slightly decreased further. When computing the O–C from the orbit, the last 3 SOFIN measurements in Table 1 show systematical deviations from the fit. They range up to 2.6 $\mathrm{km\,s^{-1}}$. Since these measurements are at a sensitive phase (close to the maximum RV, where there are also not many other measurements) they might be responsible for a large part of the eccentricity. For Solution 3, they are therefore removed from the data set. The eccentricity dropped again by a factor 2, now being only a $1\,\sigma$ result and extremely small. We thus conclude (as was already suspected by Bopp & Dempsey 1989) that the orbit is in fact circular. Solution 4 is accordingly a forced circular fit to the data set used for Solution 3 (SOFIN + Eker, excluding the last 3 measurements in Table 1) and we adopt it as the final solution. The insignificant changes in the orbit parameters and in σ_1 from Solution 3 to Solution 4 support our conclusion of circularity. Note, that the period of the final orbital solution is still based on the whole data set covering the time interval 1902–1995; only all other parameters are derived from the limited, but most accurate data. As can be seen from Table 3 the parameters are very close to those given by Bopp & Dempsey (1989).

Figure 2 shows the measurements of SOFIN and Eker (1986) together with the fit of Solution 4. The systematic deviation of the last 3 SOFIN measurements close to phase 0 is clearly seen. These and the significant deviations of a few other data points are probably caused by strong distortions of the line profiles due to spot features.

4. The rotation parameters

4.1. The rotation period

Strassmeier et al. (1993) list a rotation period for σ Gem of $P_{\mathrm{rot}} = 19.410$ days. Henry et al. (1995) analyse long–term photometric data and interpret them in a two–spot model. They obtain for each spot a different period, most of them shorter than the orbital period, which is interpreted by them as differential rotation. They give a rotation period of the star $P_{\mathrm{rot}} = 19.54$ days. Jetsu (1996) analysed the same data as Henry et al. (1995). He finds that the data of σ Gem's light minima indicate the presence of active longitudes, which means a unique period. His period is $P_{\mathrm{rot}} = (19.606 \pm 0.023)$ days. This period is identical (within the quite large errors) with the orbital period given in Eq. (5). It thus seems that σ Gem's rotation is in fact synchronized with its orbit; this is consistent also with the finding above, that the orbit is circular. We adopt in the following $P_{\mathrm{rot}} = P_{\mathrm{orb}}$.

Table 3. The results of 4 different fits of radial velocity curves to the data. Solution 1 includes all data; the errors given in parentheses are the formal fit errors, the others bootstrap errors from $B = 1000$ bootstrap runs. For Solutions 2–4, only the bootstrap errors from $B = 1000$ runs are given. Solution 2 includes only the SOFIN data supplemented by Eker's RVs (Table 1 and Table 2). Solution 3 includes the same data as Solution 2 except the last 3 SOFIN measurements. Solution 4 is a circular fit to the data used for Solution 3. For Solutions 2–4 the period was kept fixed at 19.604471 days. For comparison, the parameters given by Bopp & Dempsey (1989) are given in the column BD89

		Solution 1	Solution 2	Solution 3
P	(days)	19.604462(±0.000038)±0.000023	19.604471±0.00	19.604471±0.00
γ	($\mathrm{km\,s^{-1}}$)	44.24(±0.11)±0.11	44.28±0.14	44.47±0.14
K	($\mathrm{km\,s^{-1}}$)	34.72(±0.16)±0.16	34.73±0.19	35.04±0.19
e		0.0120(±0.0045)±0.0045	0.0109±0.0053	0.0055±0.0052
ω	(deg.)	218.36(±0.26)±23.6	240.82±23.6	281.2±38.3
T_0	(HJD)	2447224.396(±0.014)±1.283	2447225.6±1.6	2447227.8±2.1
$T_{\max}$	(HJD)	2447232.063(±0.024)±0.035	2447232.048±0.042	2447232.082±0.036
T_{conj} [1]	(HJD)	2447227.150(±0.025)±0.030	2447227.174±0.036	2447227.222±0.035
P_{rest}	(days)	19.601570(±0.00033)±0.000023	19.601575±0.000009	19.601563±0.000009
$a \sin i$	($R_\odot$)	13.445(±0.061)±0.062	13.447±0.074	13.569±0.073
$f(m)$	($M_\odot$)	0.0850(±0.0012)±0.0012	0.0850±0.0014	0.0874±0.0014
σ_1	($\mathrm{km\,s^{-1}}$)	1.53	0.99	0.89

		Solution 4	BD89
P	(days)	19.604471±0.00	19.60447±0.00007
γ	($\mathrm{km\,s^{-1}}$)	44.48±0.14	43.78±0.17
K	($\mathrm{km\,s^{-1}}$)	35.06±0.19	34.79±0.25
e		0.0±0.0	0.0210±0.0069
ω	(deg.)	0.0±0.0	160±20
T_0	(HJD)	2447232.121±0.015	2447221.2±1.1
$T_{\max}$	(HJD)	2447232.121±0.015	
T_{conj}	(HJD)	2447227.220±0.015	2447227.08±0.02
P_{rest}	(days)	19.601562±0.000009	
$a \sin i$	($R_\odot$)	13.578±0.073	13.48±0.09
$f(m)$	($M_\odot$)	0.0875±0.0014	0.0857
σ_1	($\mathrm{km\,s^{-1}}$)	0.87	

[1] Conjugation time with primary in front.

4.2. The rotation velocity

For the projected rotational velocity $v \sin i$, Eaton (1990) gives $27\,\mathrm{km\,s^{-1}}$, a value used by Hatzes (1993) and Henry et al. (1995). Strassmeier et al. (1993) give $v \sin i = 25\,\mathrm{km\,s^{-1}}$ and remark that this value is better than the one given by Eaton.

Since $v \sin i$ is a very important observable concerning the constraints to be derived in the next section and a sensitive input parameter for the forthcoming surface imaging, a redetermination seems to be necessary. For this, we use the Fourier transform of the SOFIN spectra (see e.g. Unsöld 1955; Gray 1988, p. 2–1ff).

A mean spectrum is created from all 29 SOFIN spectra. For this, each spectrum has been shifted to $\mathrm{RV_{hel}} = 0$ using the orbital parameters of Solution 4 in Table 3. In order to minimize distortions due to noise and occasional spot features, a $\kappa\,\sigma$–clipping has been done (in 3 iterations remove for each wavelength those points that are deviating more than $\kappa = 2$ times the standard deviation from the mean). The power–spectrum obtained from the whole

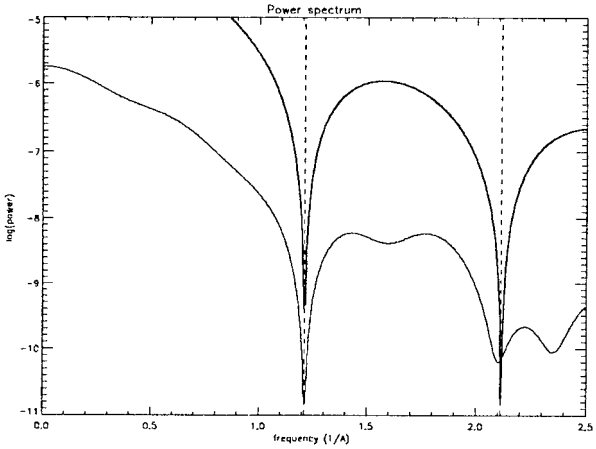

Fig. 3. Power spectrum of Fe I 6173 Å from the mean spectrum 1993-95, compared to that of a pure rotation profile computed with a linear limb–darkening of $\epsilon = 0.73$. $v \sin i$ for the model profile is $27.1\,\mathrm{km\,s^{-1}}$

wavelength range is dominated by the minima and maxima caused by the many blended lines. Only the features, whose main components are Fe I 6173 Å and Fe I 6180 Å, are sufficiently unblended to be used.

Figure 3 shows the power–spectrum obtained from Fe I 6173 Å. It is compared to that of a pure rotational profile computed with a linear limb–darkening coefficient $\epsilon = 0.73$ (obtained by interpolating to $T_{\rm eff} = 4500\,{\rm K}$, $\log g = 2.5$, $\lambda = 6175\,$Å in the tables given by Al–Naimiy 1978). It is obvious, that the second minimum is already heavily distorted by blending effects, so only the first minimum can be used (the same is true for Fe I 6180 Å). The mean projected rotational velocity determined from the two lines is

$$v \sin i = 27.0 \pm 0.2\,{\rm km\,s^{-1}}. \quad (6)$$

This is consistent with the value given by Eaton (1990) and will be used in what follows.

5. Constraints on the fundamental parameters

5.1. The minimum radius

The true rotation period $P_{\rm rot} = P_{\rm orb,rest} = 19\overset{\rm d}{.}601562$ combined with the projected rotational velocity $v \sin i = 27.0\,{\rm km\,s^{-1}}$ gives a lower limit for the radius of the star:

$$R \sin i = \frac{P_{\rm rot}}{2\,\pi}\, v \sin i = 10.5\, R_\odot. \quad (7)$$

This is only valid if the star is assumed to be spherical. Due to its relatively long rotation period it seems unlikely that the star is flattened by rotation; it might, however, approach its Roche–lobe limit and become distorted. The assumption of sphericity is thus equivalent to the assumption that the star does not fill its Roche–lobe. So far, there is no observation indicative of mass–transfer in the system, so this assumption seems to be justified. Note that here and in the following we do not distinguish between the inclination of the axis of rotation and that of the orbital axis. Since the orbit is circularized and the rotation is synchronized with the orbit it is natural to assume that these two axes are aligned. This is supported by the results of Stawikowski & Glebocki (1994).

5.2. The Roche–lobe limit

In the following the index 1 ("primary") indicates the visible component of the binary (the K1 III star) and the index 2 the secondary. The orbital parameters determine $a_1 \sin i$. If the primary would fill its Roche–lobe, the ratio of the effective radius of the Roche–lobe $R_{\rm rl}$, i.e. the radius of the sphere that has the same volume as the Roche–lobe, and the distance between the two stars, i.e. $a = a_1 + a_2 = a_1\,(1 + q)$ is entirely determined by the mass–ratio $q_{\rm rl} = m_1/m_2$ of the two components:

$$\frac{R_{\rm rl}}{a} = \frac{R_{\rm rl} \sin i}{a_1 \sin i (1 + q_{\rm rl})} = \frac{0.49\, q_{\rm rl}^{(2/3)}}{0.6\, q_{\rm rl}^{(2/3)} + \ln\left(1 + q_{\rm rl}^{(1/3)}\right)} \quad (8)$$

(Eggleton 1983). Since $R_1 < R_{\rm rl}$ and $R_{\rm rl}$ increases with $q_{\rm rl}$, we obtain a lower limit for the mass ratio q, if we replace $R_{\rm rl}$ by R_1 in Eq. (8):

$$q = \frac{m_1}{m_2} > q_{\rm rl} = 1.02. \quad (9)$$

5.3. The secondary

The mean SOFIN spectrum has been subtracted from each of the individual spectra and the residuals carefully examined. There are variations exceeding the noise, they are, however, inside the spectral features, i.e. their displacement with respect to the primary star is less than $27.0\,{\rm km\,s^{-1}}$. They cannot be due to the secondary, because from the limit of the mass-ratio it can be concluded that the displacement should reach sometimes at least $K_1 + K_2 = K_1(1 + q) > 70.8\,{\rm km\,s^{-1}}$. The variations are also not systematic over the whole 2 years period; they are thus most probably features caused by surface inhomogeneities.

Thus, even with the high–resolution, high S/N SOFIN spectra, no trace of the secondary (in this wavelength region) can be found. Since the S/N of the SOFIN spectra is generally well above 100, we can conclude, that the luminosity of the secondary does not exceed 1% of the luminosity of the primary. Adopting $M_V = 0\overset{\rm m}{.}3$ for the K1 III primary (Gray 1988, Appendix B), the secondary must be fainter than $M_V \approx 5^{\rm m}$, which would make it a main–sequence star of type G6 or later, or a compact object (white dwarf, neutron star). As a star of type G6 V or later, its mass would be less than $0.95\,M_\odot$, as a white dwarf less than the Chandrasekhar–limit of $1.4\,M_\odot$. Ayres et al. (1984) analyse the far–UV spectra of σ Gem and from the lack of any trace of a hot continuum conclude that the secondary is probably a late–type dwarf.

If we adopt for the secondary $m_2 < 0.95\,M_\odot$ and take into account the mass function from the orbital solution as well as the lower limit for the mass ratio from the Roche–limit, we obtain a stringent lower limit for the inclination:

$$\begin{aligned} \sin^3 i &= (1+q)^2 \frac{f(m)}{m_2} \\ &> (1 + \min(q))^2 \frac{f(m)}{\max(m_2)} \\ \text{i.e.} \quad i &> 46\overset{\circ}{.}2. \end{aligned} \quad (10)$$

Here, $\min(x)$ and $\max(x)$ give the minimum and maximum of all possible values for x. This limit on i is interesting, because it means that σ Gem has a high inclination of its rotational axis and is therefore suitable for surface

imaging. The value of $i = 60°$ adopted for the interpretation of photometry of σ Gem e.g. by Poe & Eaton (1985) is perfectly consistent with this limit.

5.4. The limits on the mass of the primary

If we now combine $m_2 < 0.95\,M_\odot$ with the mass function and the upper limit for the inclination, $i < 90°$, we obtain an upper limit for the mass m_1:

$$\begin{aligned} m_1 &= m_2 \cdot \left(\sqrt{\frac{m_2 \sin^3 i}{f(m)}} - 1 \right) \\ &< \max(m_2) \cdot \left(\sqrt{\frac{\max(m_2)\max(\sin^3 i)}{f(m)}} - 1 \right) \end{aligned}$$

$$\text{i.e.} \quad m_1 < 2.2\,M_\odot. \tag{11}$$

A lower limit on m_1 results from the lower limit on q and $i < 90°$:

$$\begin{aligned} m_1 &= q^3 \cdot (1+q^{-1})^2 \frac{f(m)}{\sin^3 i} \\ &> \min(q) \cdot (\min(q)+1)^2 \frac{f(m)}{\max(\sin^3 i)} \end{aligned}$$

$$\text{i.e.} \quad m_1 > 0.4\,M_\odot. \tag{12}$$

Unfortunately, this limit is not very useful: a star of such low mass would probably not have become a giant yet in the 10 Gyr or so that the Galaxy exists. Probably, the mass of the primary is larger than 1 $M_\odot$.

5.5. The primary's gravity

The surface gravity g_1 of the primary can be written as:

$$g_1 = \frac{G\,m_1}{R_1^2} - \frac{(v \sin i)^2}{R_1 \sin i}. \tag{13}$$

The last term corrects for the influence of the centrifugal force, which is $v^2 \cos\phi / R_1 = v^2 \sin i / R_1$, if we adopt as a value for the observed g_1 that in the center of the stellar disk, which is at a latitude $\phi = 90° - i$. The correction for centrifugal forces consists thus only of observables and cannot be varied.

The limits for mass, radius and mass ratio then give also limits for the surface gravity:

$$g_1 < G\frac{\max(m_1)}{\min(R_1^2)} - \frac{(v \sin i)^2}{R_1 \sin i}$$

$$\text{i.e.} \quad \log g_1 < 2.73 \tag{14}$$

$$\begin{aligned} \text{and } g_1 &= G \cdot q \cdot (1+q)^2 \frac{f(m)}{R_1^2 \sin^3 i} - \frac{(v \sin i)^2}{R_1 \sin i} \\ &> G \cdot \min(q) \cdot (1+\min(q))^2 \\ &\quad \cdot \frac{f(m)}{(R_1 \sin i)^2} \frac{1}{\max(\sin i)} - \frac{(v \sin i)^2}{R_1 \sin i} \end{aligned}$$

$$\text{i.e.} \quad \log g_1 > 1.91. \tag{15}$$

Note, that the lower limit corresponds to the lower limit for m_1, which is too low. If we assume $m_1 > 1\,M_\odot$, then

$$\begin{aligned} g_1 &= \frac{G\,m_1 \sin^2 i}{R_1^2 \sin^2 i} - \frac{(v \sin i)^2}{R_1 \sin i} \\ &> \frac{G \min(m_1) \min(\sin^2 i)}{R_1^2 \sin^2 i} - \frac{(v \sin i)^2}{R_1 \sin i} \end{aligned}$$

$$\text{i.e.} \quad \log g_1 > 2.08. \tag{16}$$

Therefore, the true gravity is very probably higher than $\log g_1 = 2$.

5.6. The mass–mass–plot of the allowed stellar parameters

In Fig. 4, the results of the previous paragraphs are presented in graphical form in the (m_1, m_2)–plane. The oblique lines to the left are the mass–ratios $q = 1.0$ (for orientation) and $q = q_{\rm rl}$. The curves are lines of constant radius of the primary, and since $R_1 \sin i$ is fixed, lines of constant inclination as well. Since the mass function is also fixed, each value of m_1 for given R_1 thus corresponds uniquely to a value of m_2. Lines $m_2 = 0.95\,M_\odot$ and $m_2 = 1.4\,M_\odot$ are also shown. Note, that if $0.95\,M_\odot < m_2 < 1.4\,M_\odot$ the secondary needs to be a white dwarf or low mass neutron star, because a main–sequence star would have been detected in the spectra, and above $1.4\,M_\odot$ it must be a neutron star. To emphasize the importance of the gravity, the lines of constant $\log g_1 = 2.0, 2.5, 3.0$ are added to the figure. We note, that the line $\log g_1 = 2.0$ is almost always above the Roche–limit $q = q_{\rm rl}$ and the line $\log g_1 = 3.0$ entirely in the region with $m_2 > 0.95\,M_\odot$. Note, that for a normal radius, $R_1 = 16\,R_\odot$ (Dyck et al. 1996), the secondary is most probably too massive to be a white dwarf.

6. Summary and discussion

New high quality radial velocity measurements of the RS CVn star σ Gem have been used to derive the orbital parameters of this single–lined binary. Essentially, the orbit given by Bopp & Dempsey (1989) is confirmed; however, the orbit is most probably circular.

The orbital parameters and the rotational parameters $P_{\rm rot} = P_{\rm orb}$ and the newly determined $v \sin i = 27.0\,{\rm km\,s^{-1}}$ (confirming the result by Eaton 1990) are combined to construct the region of allowed combinations of the inclination, the two masses and the gravity of the primary. A few plausible assumptions have to be made during this process:

- that the primary is spherical and does not fill its Roche–lobe;
- that the rotational axis of the primary and the orbital axis are parallel;
- that the secondary is less massive than $0.95\,M_\odot$.

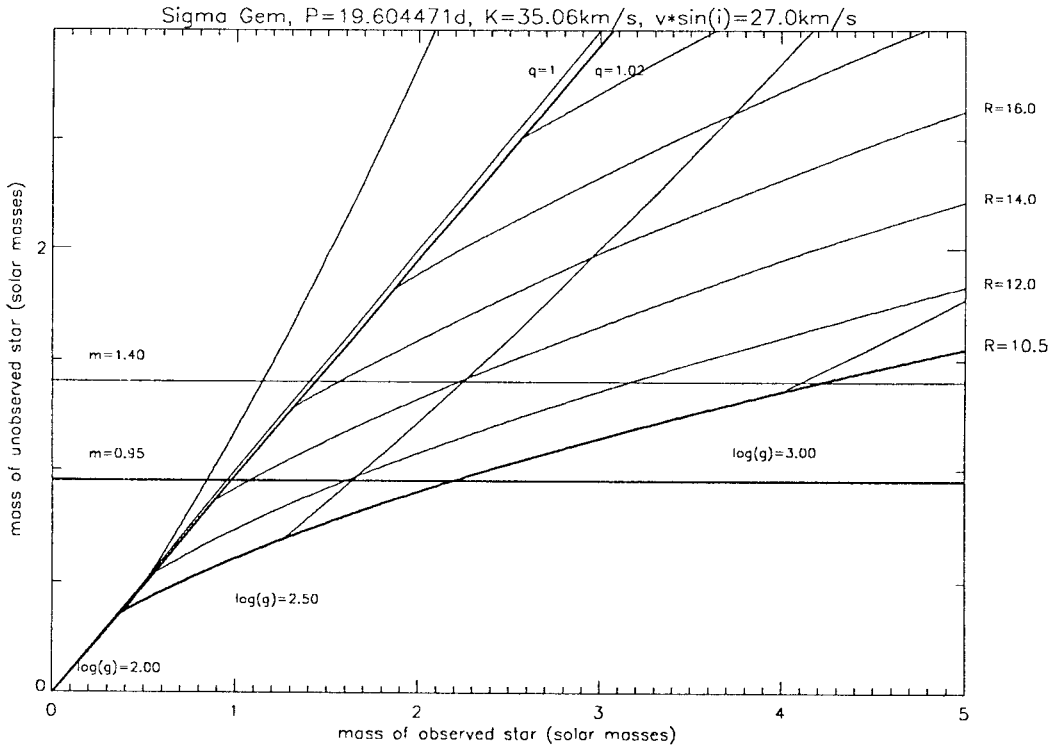

Fig. 4. The stellar parameters in the mass–mass–plane. See text for detailed explanation

The first assumption is made plausible by the fact that the RV curve is stable over the century of data, i.e. there seems to be no interaction between the components. The second assumption is based on the circularized orbit and the seemingly synchronized rotation; the third on the invisibility of the secondary in the high S/N SOFIN spectra and the additional assumption that it is a main–sequence star.

The inclination is high: $i > 46°$. The mass of the primary is between $0.4\,M_\odot$ (or more probably $1\,M_\odot$) and $2.2\,M_\odot$ which is normal for a K1–giant (Schmidt–Kaler 1982), at least when it belongs to the old disk population (Eker 1992; Eggen 1993). Its radius, however, seems to be smaller than the "normal" values for stars of this type.

The limits on the gravity are especially interesting: The gravity is in principle an observable; it can be obtained from careful modelling of the spectrum. As can be seen in Fig. 4 an accurate determination of the gravity leads to a very narrow range for the allowed values of m_1. Unfortunately, the atmospheric models are usually calculated in steps of $\delta \log g = 0.5$. Our limits here indicate, that practically the only gravity allowed is then $\log g_1 = 2.5$. The next lower gravity is almost certainly excluded, because the mass of the primary becomes too low for its spectral class or the Roche–lobe limit would be violated. Should we, however, find that a *higher* gravity is needed to describe the spectrum, this would also contradict our limits. The most uncertain assumption made is that the secondary is a main–sequence star. For a higher gravity in the primary, *both* stars have to be more massive. Since under these conditions the secondary cannot be a main–sequence star (otherwise it would have been seen at least in the SOFIN spectra) and it cannot be a white dwarf (Ayres et al. 1984) we need to conclude that the secondary had to be a neutron star. Note that this would also mean, that the primary's radius is then allowed to be at its normal value of $(16 \pm 2)\,R_\odot$ (Dyck et al. 1996, consistent with Schmidt–Kaler 1982). For $R_1 \approx 16\,R_\odot$ the inclination would only be $i \approx 41°$. This might be another check, because according to Piskunov et al. (1996) (largely) different i can be distinguished by the quality of surface imaging.

The fact that during the history of RV curves for σ Gem all new orbital solutions tend to confirm (with increasing refinement) the previous solutions is a sign that there is no interaction between the two stars. If the secondary would be a neutron star, there is therefore not much hope to see any sign of it. If, however, indirect evidence for it is found (e.g. by the necessity of a $\log g_1 \geqq 3$ to describe the spectrum), σ Gem would turn out to be indeed a very special RS CVn–star.

Acknowledgements. This work has made use of the SIMBAD data base, operated at CDS, Strasbourg, France. Z. Eker has kindly made his unpublished individual RV–measurements available to us. We thank the referee, B.W. Bopp, for his valuable comments. R.D. would like to thank A. Bruch for very

helpful discussions concerning the Roche–lobe limit; he gratefully acknowledges further discussions with S. Jankov and O. Vilhu. The project "Late–type stars: activity, magnetism, turbulence" is supported by the EC Human Capital and Mobility Network, No. ER–BCHRXCT940483.

References

Abt H.A., 1970, ApJS 19, 387
Al–Naimiy H.M., 1978, ApSS 53, 181
Ayres T.R., Simon L., Linsky J.L., 1984, ApJ 279, 197
The Astronomical Almanac for the year 1996, 1995, U.S. Government Printing Office, Washington, and HMSO, London, p. H43
Bevington P.R., 1969, Data Reduction and Error Analysis for the Physical Sciences. McGraw–Hill, New York, p. 245
Bopp B.W., Dempsey R.C., 1989, PASP 101, 516
Caceci M.S., Cacheris W.P., 1984, Byte 9, 340
Dyck H.M., Benson J.A., van Belle G.T., Ridgway S.T., 1996, AJ 111, 1705
Eaton J.A., 1990, IBVS 3460
Efron B., Tibshirani R.J., 1993, An Introduction to the Bootstrap. Chapman & Hall, New York
Eggen O.J., 1993, AJ 106, 80
Eggleton P.P., 1983, ApJ 268, 368
Eker Z., 1986, MNRAS 221, 947
Eker Z., 1992, ApJS 79, 481
Gray D.F., 1988, Lectures on Spectral–Line Analysis: F, G, and K Stars. The Publisher, Arva, Ontario
Harper W.E., 1914, Publ. Dom. Obs. Ottawa 1, 265
Harper W.E., 1935, Publ. Dom. Astrophys. Obs. Victoria 6, 207 (see p. 224)
Hatzes A.P., 1993, ApJ 410, 777
Heintz W.D., 1978, Double Stars. Reidel, Dordrecht, p. 80
Henry G.W., Eaton J.A., Hamer J., Hall D.S., 1995, ApJS 97, 513
Ilyin I.V., 1996, latest edition of Acquisition, Archiving and Analysis (3A) Software Package – User's Manual, Observatory, University of Helsinki
Jetsu L., 1996, A&A 314, 153
Jones H.S., 1928, Ann. Cape Obs. 10, pt. 8 (see p. 170)
Lunt J., 1919, ApJ 50, 161
Mackay C.D., 1986, ARA&A 24, 255
Moore J.H., 1928, Publ. Lick Obs. 16 (see p. 117)
Pierce A.K., Breckinridge J.B., 1973, The Kitt Peak Table of Photographic Solar Spectrum Wavelengths, Kitt Peak Contr. No. 559
Piskunov N., Ryabchikova T.A., Tuominen I., 1996, A&A (submitted)
Poe C.H., Eaton J.A., 1985, ApJ 289, 644
Press W.H., Teukolsky S.A., Vetterling W.T., Flannery B.P., 1994, Numerical Recipes in C. Cambridge Univ. Press, Cambridge, 2nd ed., 2nd repr., p. 408ff
Reese H.M., 1903, ApJ 17, 308
Schmidt–Kaler T., 1982, in Landolt–Börnstein, New Series, Group VI, Vol. 2b, p. 1
Stawikowski A., Glebocki R., 1994, Acta Astron. 44, 393
Strassmeier K.G., Hall D.S., Fekel F.C., Scheck M., 1993, A&AS 100, 173
Tuominen I., 1992, NOT News, No. 5, p. 15
Unsöld A., 1955, Physik der Sternatmosphären. 2nd ed., Springer, Berlin, p. 513
Willmarth D., 1987, A CCD Atlas of Comparison Spectra: Thorium–Argon Hollow Cathode, Kitt Peak National Observatory, revised 1992